Vol. 46 (2015) ACTA PHYSICA POLONICA B No 5

DISSIPATIVE ORBITING IN ^{136}Xe+^{209}Bi REACTIONS AT 28 AND 62 AMeV

W. Gawlikowicz

Faculty of Biology and Environmental Sciences
Cardinal Stefan Wyszyński University
Dewajtis 5, 01-815 Warszawa, Poland

J. Błocki

National Centre for Nuclear Research, Hoża 69, 00-681 Warszawa, Poland

T. Barczyk, K. Grotowski, S. Micek, R. Płaneta
A. Wieloch, Z. Sosin

The Marian Smoluchowski Institute of Physics, Jagiellonian University
Łojasiewicza 11, 30-348 Kraków, Poland

(Received July 28, 2014; revised version received November 3, 2014; final version received April 30, 2015)

Correlations between the energy, charge and the deflection angle of the projectile-like fragments were studied for the ^{136}Xe + ^{209}Bi reaction at E/A = 28 and 62 MeV. These correlations are seen to exhibit features characteristic of dissipative orbiting, commonly found at bombarding energies of a few MeV/nucleon above the interaction barrier, but also reported in the Fermi-energy domain. It was found, that in the studied bombarding energy range, the reaction cross section is still dominated by the dissipative binary reactions of well defined projectile- and target-like fragments.

DOI:10.5506/APhysPolB.46.1025
PACS numbers: 25.70.Pq, 25.70.Mn

1. Introduction

In recent years, a considerable effort has been made to explore heavy-ion reaction dynamics. At low bombarding energies, the collisions are governed by the interplay of the repulsive Coulomb and attractive nuclear mean-field interactions, with one-body dissipation largely responsible for the dissipation

of the initial kinetic energy into the thermal energy [1]. At high energies (few hundreds MeV/nucleon), on the other hand, the collision dynamics is largely governed by nucleon–nucleon interactions, with the repulsive part of the nuclear mean field and two-body dissipation playing dominant roles [2]. The reaction mechanism is, hence, expected to undergo significant changes at intermediate bombarding energies of few tens of MeV/nucleon [3].

Comparing reaction pictures for low and high bombarding energies, one can find that the heavy-ion reactions at intermediate bombarding energies (20–100 MeV/nucleon) have features characteristic for low bombarding energies as well as those for high bombarding energies. This fact makes Fermi bombarding energies an interesting research region. It makes it also difficult to interpret.

The interplay between one- and two-body dissipation in intermediate energy collisions is well demonstrated by the balance energy concept [4]. It corresponds to bombarding energy where the attractive scattering is balanced by repulsive scattering. At low bombarding energies, the attractive mean-field interaction results in negative scattering angles related to the orbiting of the transient dinuclear complex. At high bombarding energies, one can neglect mean-field effects. The dominating two-body nucleon–nucleon interaction results in positive scattering angles.

The study of correlations between the energy and the deflection angle of projectile-like fragments (PLF) has played a crucial role in gaining the understanding of the heavy-ion reaction dynamics both, at low bombarding energies of a few MeV/nucleon above the interaction barrier [5] and at lower boundary of the intermediate collisions energy region [6]. It has been shown [6] that for this latter energy domain (28 MeV/nucleon), the reaction cross section is still dominated by dissipative binary reactions involving well defined projectile- and target-like fragments, similar to what is observed at low bombarding energies [5].

The present study reveals that such dissipative orbiting of dinuclear systems composed of well-defined projectile- and target-like fragments is a common reaction scenario for bombarding energies as high as 62 MeV/nucleon.

2. Experimental setup

The experiments were performed at the National Superconducting Cyclotron Laboratory of the Michigan State University. Beams of ^{136}Xe ions with energies 28, 40 and 62 MeV/nucleon were focused on a self-supporting 3.5 mg/cm^2 thick ^{209}Bi targets.

The experimental setups included, in every case, two 4π detector systems: *(i)* the Washington University charged-particle detector array — Dwarf Ball/Wall [7], *(ii)* the University of Rochester neutron calorimeter

RedBall for 28 MeV/nucleon study, and the SuperBall neutron multiplicity meter [8] for 40 and 62 MeV/nucleon studies. The data measured by Dwarf Ball/Wall and SuperBall detectors are presented elsewhere [9].

Here, we want to focus on experimental data obtained for energies 28 and 62 MeV/nucleon, measured by silicon-detector telescopes placed at very forward angles, including the angular region around the grazing angle. The PLF telescopes were position sensitive, allowing for an accurate measurement of the PLF emission angle, anticipating the reaction grazing angle — θ_{det}= 4.48° and 2.91°, for 28 and 62 MeV/nucleon reactions, respectively.

The experimental set-up emulator including detection thresholds and detectors geometry was applied in order to allow proper comparison between the experimental and model data.

The preliminary data measured by the PLF telescopes were already presented in conference contribution [10].

3. Theoretical modeling

In heavy-ion reactions, the fundamental theoretical modeling itself is typically a two-step process, with the first step aiming at describing the collision dynamics and the second one aiming at describing the decay of the primary reaction products. Therefore, two theoretical codes were used alternately to model the dynamical interaction stage of the collision, while the equilibrium-statistical decay code GEMINI [11] was used to model the subsequent statistical decay of the primary products emerging from the interaction stage.

The interaction stage was modeled using either: *(i)* the Quantum Molecular Dynamics (QMD) code CHIMERA [12], or *(ii)* the deterministic classical model based on the Rayleigh–Lagrange equations of motion [13].

The one-body dissipation used in the Rayleigh–Lagrange classical approach means a chaotic excitation of a gas of independent particles due to their interaction, with a time-dependent mean field potential. The two-body dissipation corresponds to the particle–particle collisions inside the "container".

In the QMD calculations, the time-evolution of the system reflects the propagation of *wave packets* associated with nucleons [12], and is assumed to be governed by the Ritz variational principle [14], what is equivalent to solving the classical Hamiltonian equations of motion for centroids of wave packets.

The QMD model includes also a simulation of nucleon–nucleon collisions, related to the nucleon–nucleon cross section, σ_{NN}, which is energy and isospin dependent [15]. Any two nucleons are considered candidates for

a collision, whenever their spatial separation, r_{ij}, is smaller than the distance determined by the nucleon–nucleon cross section

$$r_{ij} < \sqrt{\sigma_{NN}/\pi}\,. \tag{1}$$

It is then assumed that a collision actually takes place then and only then when the final nucleonic states of the probed candidate collision are not occupied by nucleons of the same kind (Pauli blocking).

The advantage of molecular dynamics approach is the possibility of calculating dynamics of all individual nucleons what introduces properly the particle–particle correlations. It gives also a possibility of simulating the pre-equilibrium emission, and more importantly, the dynamical fragment emission in the early stage of a collision.

The version of the CHIMERA code used here [12] included isospin-dependent nuclear interactions, and calculations were performed for the time interval from 0 up to 300 fm/c assuming a soft equation of state ($K \approx 200$ MeV) with symmetry energy strength coefficient corresponding to an ASY-STIFF equation of state ($C = 31.4$ MeV) [16].

In this contribution, the Rayleigh–Lagrange Classical Model (RLCM) calculations were performed where only the one-body dissipation was used [17].

The idea of the classical model is the following — we are solving numerically a set of the generalized Lagrange equations

$$\frac{d}{dt}\frac{\partial L}{\partial \dot{q}_i} + \frac{\partial F}{\partial \dot{q}_i} = \frac{\partial L}{\partial q_i}\,, \tag{2}$$

where $L(q_i, \dot{q}_i) = T(q_i, \dot{q}_i) - V(q_i)$ is the Lagrangian of the system and $F(q_i, \dot{q}_i)$ is the Rayleigh dissipation function, where one-body dissipation was assumed. Hence, in the first stage of reaction, there are two colliding Fermi gases, for which the "window" formula is effective, while in the later stage, when colliding nuclei slow down, most effective becomes the "wall" formula.

For q_i, we have taken three essential for our problem coordinates, namely a separation coordinate ρ, a neck coordinate λ and a mass asymmetry coordinate Δ. These three coordinates define completely our volume conserving axially symmetric shapes which consist of two generally unequal spheres joined smoothly by a quadratic surface of revolution [18]. For the kinetic energy T, a quadratic form in $\dot{\rho}, \dot{\lambda}$ is used. In the dynamical calculations, we have found that the motion in Δ direction is strongly overdamped to such an extent that we can safely neglect the kinetic energy motion associated with $\dot{\Delta}$. For the mass tensor, a Werner–Wheeler approximation [19] to the hydrodynamical mass is used. The potential energy V is calculated as a sum of the nuclear part and the Coulomb part. For the nuclear part, we adopt

a double folding procedure developed by Krappe, Nix, Sierk [20] and in the Coulomb part, we take into account corrections for the diffuseness of the charge distribution.

The differences in the applied theoretical modeling are well illustrated in Fig. 1, where the calculated excitation energy per nucleon of *primary* PLF is presented as a function of (model) normalized impact parameter. As one can see, the difference in the predicted excitation energy of the primary PLF, grows with increasing bombarding energy.

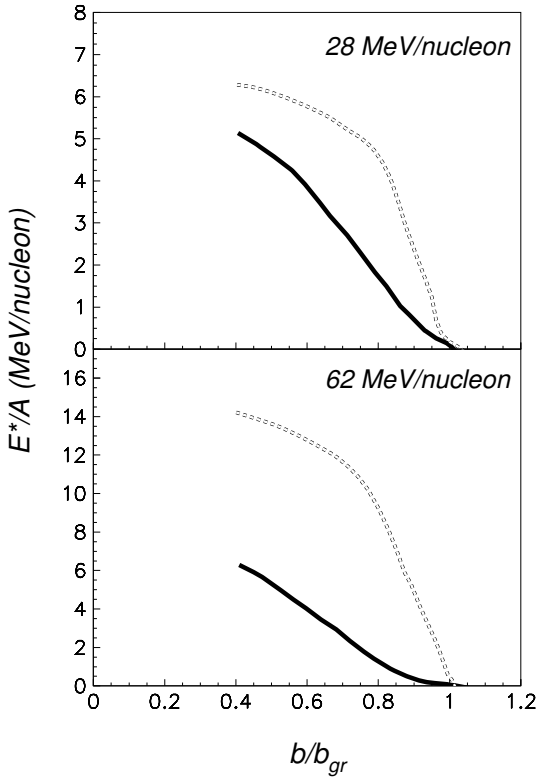

Fig. 1. Excitation energy per nucleon of *primary* PLF as a function impact parameter, normalized to corresponding grazing angle value. Solid line — QMD model. Broken line — RLCM model.

The increase of the PLF excitation energy in the Rayleigh–Lagrange Classical Model, as compared to QMD calculations, is mainly due to the fact that in the RLCM calculations the dynamical and pre-equilibrium emission in the early collision phase is neglected. Consequently, more excitation is available for PLF and TLF fragments. However, one should also take into account the differences in the colliding system shape evolution, predicted by

the QMD and RLCM models. This means that the available energy can be distributed in different fashion, including the collective degrees of freedom as angular momentum of the system and the spins of fragments.

4. Dissipative orbiting

The logarithmic contour plots of PLF energy as a function of PLF deflection angle, obtained for QMD calculations, are displayed in Fig. 2, for bombarding energies of $E/A = 28$ and 62 MeV. The final deexcitation was simulated with equilibrium-statistical decay code GEMINI. Figure 2 presents also several characteristic system trajectories representing elastic (1), grazing (2), moderately damped (3), and negative-angle, orbiting-like (4) collisions. The segments of the deflection-function plots corresponding to these four classes of trajectories are labeled 1 through 4.

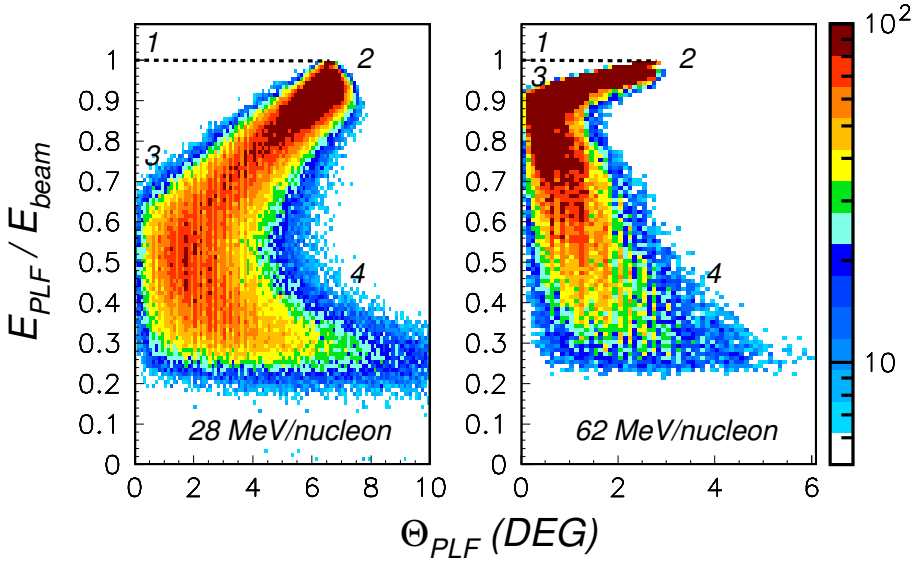

Fig. 2. (Color online) Logarithmic contour plots of measured PLF energy, normalized to beam energy ($E_{\mathrm{PLF}}/E_{\mathrm{beam}}$), as a function of detected PLF angle (Θ_{PLF}), as obtained from QMD simulation with deexcitation phase simulated by equilibrium-statistical decay code GEMINI. The broken lines show results for elastic and quasi-elastic reactions.

As seen in Fig. 2, sections of the yield ridges associated with elastic scattering connect regions labeled 1 and 2. For mid-peripheral collisions, the two colliding heavy ions form a transient dinuclear system and orbit about each other for a fraction of a revolution, while dissipating some of their relative kinetic energy. This process is reflected in segments 2–3 and 3–4 of the

yield ridges. For the segment connecting areas 2 and 3, the PLF deflection angle is seen to decrease with increasing energy dissipation, reflecting the fact that both, the energy dissipation and the deflection angle are functions of the impact parameter and that with decreasing impact parameter, the former increases, while the latter decreases. For the segment connecting regions 3 and 4, on the other hand, the deflection angle is seen to increase with increasing energy dissipation and, hence, decreasing impact parameter. One should note that the experiment is unable to distinguish negative-angle deflection from that due to positive angles. Therefore, the plots are showing only positive angles. It is worth noting that there is no conceptual difference between dissipative orbiting leading to either positive or negative deflection angles. The angle of zero degrees plays no special role, except that it gives a reflection of a part of the plot which, using negative angles convention, would appear at negative angles — see Fig. 2.

Similar behavior can be observed using the correlation between the PLF charge and its emission angle — see Fig. 3. The general agreement in reaction picture in view of Figs. 2 and 3 is due to strong correlation between the measured PLF charge and its energy — the kinetic energy loss of PLF is mainly due to loss of its mass (charge) during the deexcitation phase.

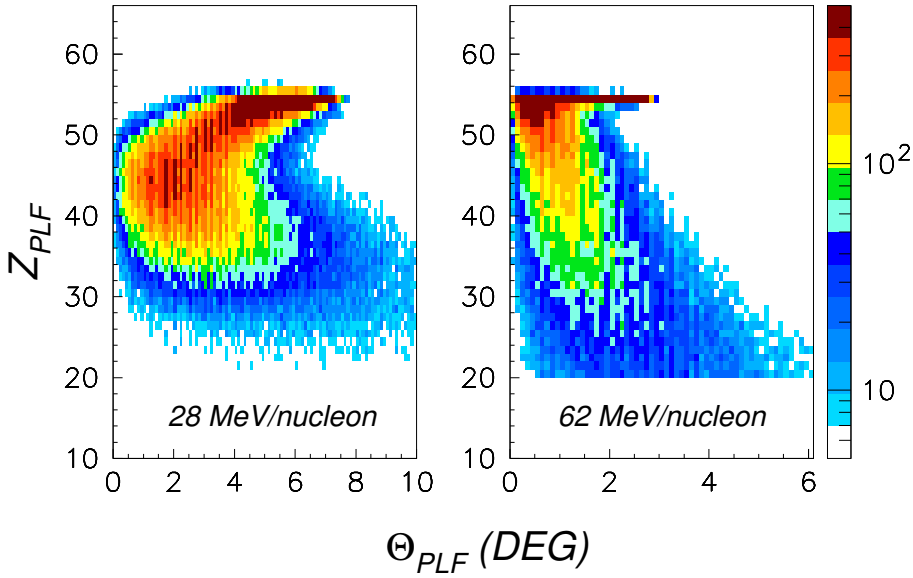

Fig. 3. (Color online) Logarithmic contour plots of the PLF charge (Z_{PLF}) as a function detected PLF angle (Θ_{PLF}) in LAB system representation, for bombarding energy 28 and 62 MeV/nucleon, as obtained from QMD simulation with deexcitation phase simulated by equilibrium-statistical decay code GEMINI.

The crest lines of theoretical distributions "filtered" through experimental set-up emulator are presented in Figs. 4 and 5, together with experimentally measured correlations for the Xe+Bi reaction at bombarding energies 28 and 62 MeV/nucleon. As one can see, the crest lines of model calculations indicate consistency with trends observed in experimental data, reproducing general "topography" of the yield ridges.

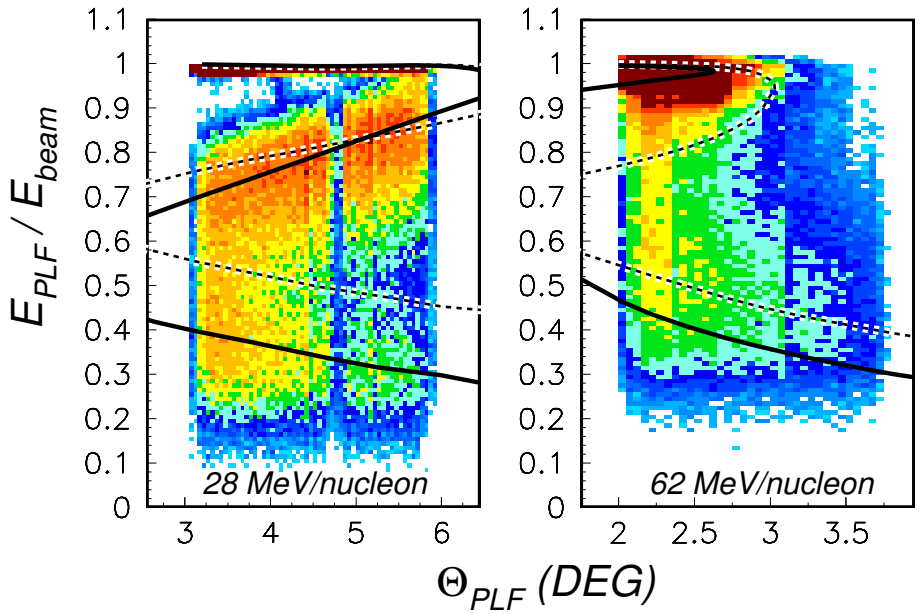

Fig. 4. (Color online) Comparison of logarithmic contour plots of measured PLF energy, normalized to beam energy ($E_{\mathrm{PLF}}/E_{\mathrm{beam}}$), as a function of detected PLF angle (Θ_{PLF}), with the results of model calculations (LAB system). Solid line — QMD model. Broken line — RLCM calculations. Deexcitation phase simulated by equilibrium-statistical decay code GEMINI. Experimental set-up emulator was used for theoretical data.

The best agreement with experimental data was obtained for QMD simulation. As can be seen in Figs. 4 and 5, the RLCM calculations underestimate the PLF energy and charge loss, for high dissipation region associated with mid-central or central collisions (lower branch in left and right panels). This underestimation can be explained as an effect of absence of two-body dissipation, playing important role in this collision region.

More complicated situation can be found in the upper branches seen in Figs. 4 and 5. In principle, one-body dissipation model should properly reproduce experimental data in this region, since for peripheral collisions

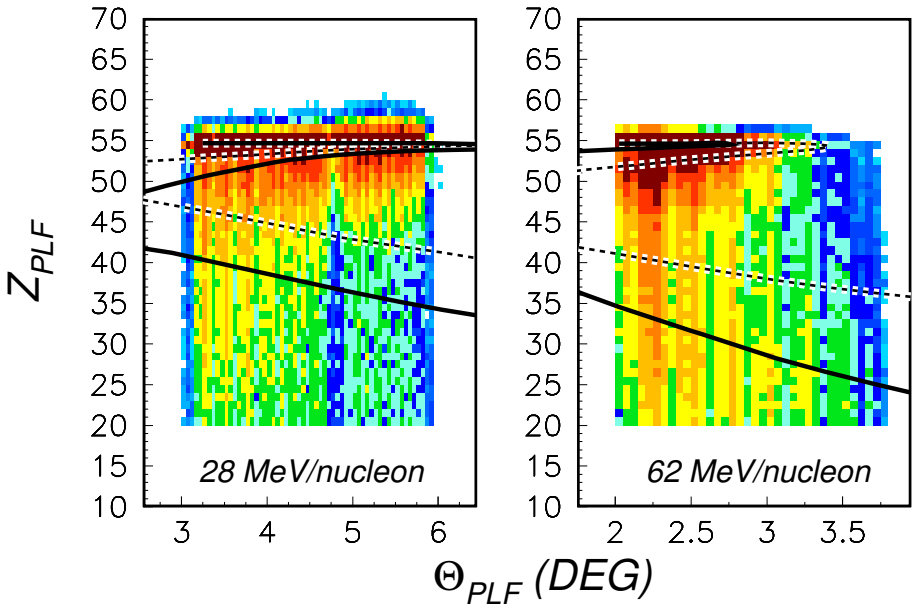

Fig. 5. (Color online) Comparison of logarithmic contour plots of measured PLF charge (Z_{PLF}) as a function of detected PLF angle (Θ_{PLF}), with model calculations (LAB system). Solid line — QMD model. Broken line — RLCM calculations. Deexcitation phase simulated by equilibrium-statistical decay code GEMINI. Experimental set-up emulator was used for theoretical data.

two-body dissipation should have a week influence. Here, a possible explanation of the observed discrepancy can be connected with RLCM model assumptions.

The main assumption made in deducing one-body dissipation formula is that the velocity of the "container wall" is small as compared to the average velocity of nucleons. This is not the case, especially at 62 MeV/nucleon, where the velocity of "walls" is comparable to the Fermi velocity. Consistently, one can find a rather good agreement between results of the calculations for the upper branch of the experimental data for 28 MeV/nucleon, where this assumption is more fulfilled than for 62 MeV/nucleon (see Fig. 4). Therefore, the applicability of the RLCM model in the case of 62 MeV/nucleon is rather questionable.

One should also take into account, that QMD and RLCM models simulate the primary reaction scenario, while the final energy and charge loss of PLF is mainly due to subsequent deexcitation phase simulated by the GEMINI code (see also Fig. 1).

Generally, as it appears from Figs. 4 and 5 that the collision scenario, as the one of dissipative orbiting with a subsequent statistical decay of the primary PLF and TLF, is essentially the same at $E/A = 62$ MeV as it was earlier found at lower bombarding energies. Like it is the case for lower bombarding energies, at $E/A = 62$ MeV, most of the reaction cross section is still associated with binary collisions, where the term "binary" refers to the primary collision phenomenology and not to the number of reaction products actually observed. In view of the above, the transition to a high-energy scenario dominated by two-body interactions and two-body dissipation must be occurring at higher bombarding energies than $E/A = 62$ MeV.

The comparison between the QMD and RLCM models shows how sensitive is the deflection function for different model calculations. It allows to test general model assumptions used for reaction mechanisms modeling. Especially in the region of high degrees of energy dissipation (midcentral or central collisions), nucleon–nucleon collisions are expected to play an important role. In the region of more violent nuclear collisions, the general model assumptions have to be carefully validated since a binary dissipative first reaction stage might not be well separated in time from the subsequent statistical decay of primary PLFs and TLFs.

5. Summary and conclusions

The observed correlations between the energy, charge and the deflection angle of projectile-like fragment reveal that for intermediate energies as high as $E/A = 62$ MeV, the general reaction scenario is similar to that observed and understood for low energies in terms of dissipative binary collisions. Thus, at $E/A = 62$ MeV, the reaction cross section appears still dominated by dissipative binary reactions involving the survival of well-defined projectile- and target-like fragments. Consequently, the transition in reaction dynamics expected to occur at intermediate bombarding energies must be occurring at bombarding energies even higher than these used in the present study.

The projectile-like fragment deflection angle correlations have shown high sensitivity to the details of the reaction modeling. This sensitivity can be used for model verifying, especially that such type of correlations are easy to measure with very good statistics, using relatively simple experimental set-up.

This work was supported by the Cardinal Stefan Wyszyński University, Grant No. UmoPBBNS-10/14.

REFERENCES

[1] W.J. Swiatecki, *Phys. Scr.* **24**, 113 (1981).

[2] P. Danielewicz *et al.*, *Phys. Rev.* **C38**, 120 (1988).

[3] *E.g.*: H.M. Xu, *Phys. Rev. Lett.* **67**, 2769 (1991).

[4] G.D. Westfall *et al.*, *Phys. Rev. Lett.* **71**, 1986 (1993); C.A. Ogilvie *et al.*, *Phys. Rev.* **C42**, R10 (1990).

[5] *E.g.*: W.U. Schröder, J.R. Huizenga, *Treatise on Heavy-Ion Science*, Plenum Press, New York and London 1984, Vol. 2, pp. 113–726.

[6] S.P. Baldwin *et al.*, *Phys. Rev. Lett.* **74**, 1299 (1995).

[7] D.W. Stracener *et al.*, *Nucl. Instrum. Methods* **A294**, 485 (1990).

[8] W.U. Schröder, REPORT DOE/ER/79048-1, 1995.

[9] W. Gawlikowicz *et al.*, *Phys. Rev.* **C81**, 014604 (2010).

[10] W. Gawlikowicz *et al.*, Proceedings of the 11$^{\text{th}}$ International Conference on Reaction Mechanisms, Varenna 2006, p. 261.

[11] R.J. Charity *et al.*, *Nucl. Phys.* **A483**, 391 (1988).

[12] J. Łukasik *et al.*, *Phys. Rev.* **C55**, 1906 (1997).

[13] J. Blocki, H. Feldmeier, W.J. Swiatecki, *Nucl. Phys.* **A459**, 145 (1986).

[14] J. Aichelin, *Phys. Rep.* **202**, 233 (1991).

[15] K. Chen *et al.*, *Phys. Rev.* **166**, 949 (1968).

[16] B.A. Li, L.-W. Chen, C.M. Ko, *Phys. Rep.* **464**, 113 (2008).

[17] J. Blocki *et al.*, *Ann. Phys.* **113**, 330 (1978).

[18] J. Blocki, W.J. Swiatecki, report LBL-12811, 1982.

[19] I. Kelson, *Phys. Rev.* **B136**, 1667 (1964).

[20] H. Krappe, J.R. Nix, A.J. Sierk, *Phys. Rev.* **C20**, 992 (1979).